Timing of global crustal metamorphism on Vesta as revealed by high-precision U–Pb dating and trace element chemistry of eucrite zircon

Tsuyoshi Iizuka [a,b,*], Akira Yamaguchi [c,d], Makiko K. Haba [c], Yuri Amelin [b], Peter Holden [b], Sonja Zink [b], Magdalena H. Huyskens [b], Trevor R. Ireland [b]

[a] *Department of Earth and Planetary Science, The University of Tokyo, Hongo 7-3-1, Bunkyo, Tokyo 113-0033, Japan*
[b] *Research School of Earth Sciences, The Australian National University, Canberra, ACT 0200, Australia*
[c] *National Institute of Polar Research, Tokyo, Japan*
[d] *Department of Polar Science, School of Multidisciplinary Science, Graduate University for Advanced Sciences, Tokyo, Japan*

A B S T R A C T

Non-cumulate eucrites represent basaltic crust that experienced a complex thermal history involving multistage metamorphism and metasomatism, probably on asteroid Vesta. To better constrain the thermal history of these rocks and their parent body, we have integrated high-precision U–Pb age and trace element data for zircon grains with sizes up to 80 μm in the eucrite Agoult. All analyzed zircon grains yielded concordant U–Pb dates that correspond to the precise $^{207}Pb/^{206}Pb$ age of 4554.5 ± 2.0 Ma. The Ti contents in these zircon grains indicate their crystallization at subsolidus temperatures of ca. 900°C, which are similar to the inferred conditions of pyroxene exsolution in most basaltic eucrites that occurred during protracted thermal metamorphism. The zircon crystallization temperatures, together with the presence of baddeleyite needles and variable Zr concentration in Agoult ilmenite grains, indicate metamorphic origin of the Agoult zircon through Zr release from ilmenite followed by reaction with silica. We therefore consider the zircon $^{207}Pb/^{206}Pb$ age as the timing of the widespread thermal metamorphism in Vesta's crust. The metamorphic age is coincident with the oldest Mn–Cr date for cumulate eucrites, supporting the view that the thermal metamorphism is a result of burial of basaltic crust and subsequent heating from the hot interior rather than collision of asteroids. The zircon rare earth element patterns with restricted Ce positive anomalies suggest that the metamorphism occurred at an oxygen fugacity below the iron–wüstite buffer, implying the absence of oxidizing agents such as aqueous fluid within the crust at that time.

© 2014 Elsevier B.V. All rights reserved.

1. Introduction

Eucrites are the most common achondrites that are derived from pigeonite-plagioclase basaltic or gabbroic crust formed on differentiated asteroids in the early solar system (e.g., Righter and Drake, 1997). Eucritic clasts often co-exist with clasts of diogenites composed mainly of orthopyroxene and olivine, forming polymict breccias called howardites. The co-existence of eucrites and diogenites, together with their mineralogical, geochemical and isotopic signatures, suggests the genetic relationship between these two types of meteorites (e.g., Duke and Silver, 1967; Wänke et al., 1973; Clayton et al., 1976; Takeda and Mori, 1985; Warren, 1985; Drake, 2001). Spectroscopic and geochemical studies suggested that the howardite–eucrite–diogenite (HED) meteorites have originated on asteroid Vesta (McCord et al., 1970; Larson and Fink, 1975; Consolmagno and Drake, 1977; Binzel and Xu, 1993; Ruzicka et al., 1997; Burbine et al., 2001). This inference is convincingly supported by new mineralogical, geochemical and geophysical data obtained by NASA's Dawn mission at Vesta (De Sanctis et al., 2012; Russell et al., 2012; McSween et al., 2013). Thus, the eucrites offer a unique opportunity to investigate the petrogenesis and nature of crust on a planetesimal whose size, morphology and internal structure are known (Jaumann et al., 2012; Russell et al., 2012; Clenet et al., 2014). Yet decoding the primary feature and early evolution of Vesta's crust from eucrites is no easy task because most of the eucrites experienced a complex geologic history such as metamorphism, multiple impact events and/or metasomatism

---

(e.g., Takeda and Graham, 1991; Metzler et al., 1995; Yamaguchi et al., 1996, 2001; Bogard and Garrison, 2003; Barrat et al., 2011; Warren et al., 2014).

Zircon, a common accessory phase in intermediate-felsic igneous rocks and high-grade metamorphic rocks, can be precisely dated by the U–Pb chronometer. Due to its robustness zircon can retain primary chemical signatures through post-crystallization processes, some of which can reveal conditions of the zircon crystallization. For instance, Ti content in zircon is a measure of its crystallization temperature (Watson and Harrison, 2005; Watson et al., 2006), whereas the magnitude of Ce enrichment relative to neighboring La and Pr is a function of the oxidation state (Trail et al., 2011, 2012; Burnham and Berry, 2012). Accordingly, zircon is a suitable mineral for retrieving the primary chemical features of samples having a complex geologic history. Indeed, zircons from lunar samples have provided valuable insights into the timing and nature of the earliest magmatism on the Moon, despite their experience of intense impact events (e.g., Nemchin et al., 2009; Taylor et al., 2009; Grange et al., 2011; Valley et al., 2014).

Compared to lunar rocks, eucrites generally contain less abundant and smaller (<20 μm) zircon grains because eucrites have mafic bulk compositions with relatively low Zr abundances and, therefore, Zr saturation is rarely achieved (Hirata, 2001; Misawa et al., 2005; Roszjar et al., 2011, 2014; Zhou et al., 2013). Among the eucrites, higher-grade metamorphic ones tend to have larger zircon grains probably due to zircon growth during high-temperature metamorphism (Haba et al., 2014). The eucrite zircon grains were analyzed by the ion microprobe technique for U–Pb dating and yielded $^{207}Pb/^{206}Pb$ dates between 4560 Ma and 4530 Ma with uncertainties of $\pm \geq 5$ Ma (Ireland and Bukovanska, 2003; Misawa et al., 2005; Zhou et al., 2013). Notably, these zircon $^{207}Pb/^{206}Pb$ dates are older than those obtained from other phases in eucrites such as pyroxene and plagioclase (4.54–4.40 Ga, Manhes et al., 1984; Tera et al., 1997; Iizuka et al., 2013), reinforcing the utility of zircon for studying the earliest evolution of Vesta's crust. More precise ($\pm \geq 1.6$ Ma) but relative ages of eucrite zircons were estimated by the Hf–W chronometer (Ireland and Bukovanska, 2003; Srinivasan et al., 2007; Roszjar et al., 2012). The oldest eucrite zircon Hf–W date obtained for the eucrite Asuka (A)-881388 corresponds to an absolute age of 4564.0 ± 1.6 Ma when the angrite D'Orbigny is used as a time anchor (U–Pb age, Brennecka and Wadhwa, 2012 after Amelin, 2008; Hf–W, Kleine et al., 2012, all short-lived isotopic dates in this paper are referenced to D'Orbigny), whereas zircon grains in the eucrite Elephant Moraine (EET) 90020 show no resolvable W isotopic variations, suggesting its crystallization or age resetting later than 4533 Ma.

We have found that the eucrite Agoult, an unbrecciated eucrite with granulitic textures (Yamaguchi et al., 2009), contains exceptionally large zircon grains with sizes up to ∼80 μm (Fig. 1). These large grains allow us to conduct the first comprehensive chronological, geochemical and isotopic study on eucrite zircon. In this contribution, we report high-precision U–Pb dating and trace element chemistry of the Agoult zircon. The results place new constraints on the early thermal history of Vesta's crust.

2. Sample and methods

Agoult is a Saharan find, fine-grained monomict eucrite with no chemical evidence of terrestrial weathering (Barrat et al., 2003). It shows a relict subophitic texture composed of granular pyroxenes (∼80 μm in size) and elongated plagioclase (∼50 × 300 μm) with abundant ca. 120° triple junction and curved grain boundaries, indicating that a basaltic protolith has experienced high-grade metamorphism accompanied by significant recrystallization (Yamaguchi et al., 2009). The plagioclase has an anorthite content of 89 mol%, whereas the pyroxenes are homogeneous low-Ca pyroxene and augite grains (Yamaguchi et al., 2009). Minor phases are ilmenite, spinels (Ti-chromite and Cr-ulvöspinel), troilite, tridymite, Ca-phosphate, zircon and baddeleyite. In many cases, spinels are closely associated with ilmenite and troilite.

Oxygen isotopic analysis of Agoult (Yamaguchi et al., 2009) plots on the eucrite fractionation line defined by Greenwood et al. (2005). Agoult, as well as some highly metamorphosed eucrites, exhibits rare earth element (REE) patterns with light REE (LREE) depletion and Eu positive anomalies (Barrat et al., 2003; Yamaguchi et al., 2009). The REE patterns differ from common Main-Group basaltic eucrites and are akin to those of cumulate eucrites, although Agoult is similar to normal basaltic eucrites in mineral chemistry. Such unusual REE patterns of highly metamorphosed basaltic eucrites have been interpreted to reflect partial melting with subsequent melt extraction during high-temperature metamorphism (Yamaguchi et al., 2009).

Pyroxene and plagioclase fractions of Agoult were precisely dated with the U–Pb method using isotope dilution-thermal ionization mass spectrometry (ID-TIMS) (Iizuka et al., 2013). The plagioclase fractions yielded an isochron $^{207}Pb/^{206}Pb$ date of 4532.2 ± 1.0 Ma and the weighted average of model $^{207}Pb/^{206}Pb$ dates of 4532.4 ± 0.8 Ma, whereas the pyroxene fractions gave scattered data with model $^{207}Pb/^{206}Pb$ dates ranging from 4529 to 4523 Ma, indicating Pb isotopic disturbance in the Agoult pyroxene.

The zircon in the Agoult meteorite typically occurs in association with ilmenite, spinels, tridymite and/or troilite in the mesostasis (Fig. 1). The zircon grains are euhedral to subhedral and have aspect ratios of 1 to 3 with lengths of up to 80 μm. These grains are morphologically distinct from zircon grains in non-granulitic eucrites, which generally have irregular shapes and sizes smaller than 20 μm (Misawa et al., 2005; Zhou et al., 2013; Haba et al., 2014). Back-scattered electron and cathodoluminescence imaging show no clear zoning structure in the Agoult zircon grains (Fig. 2). In this study, trace element data were obtained *in situ* from eleven separate spots on seven zircon grains in three thin sections. We further performed high-precision ID-TIMS U–Pb dating on eight zircon grains, including the five grains analyzed for trace element concentrations, extracted from five thin sections.

Determination of trace element abundances was carried out on the SHRIMP RG ion microprobe at the Australian National University (ANU). A ∼1.5 nA primary O_2^- beam was focused into a spot ∼20 μm diameter on the sample surface coated with gold. The mass spectrum between masses 45 and 254 is deconvolved into Zr, Ti, Si, Y, Nb, La, Ce, Pr, Nd, Sm, Eu, Gd, Dy, Hf, Pb and U atomic and/or monoxide species and counts for each ions were normalized to SiO_2^+. We utilized a relatively high mass resolution of ∼12,000 at 1% peak height to resolve interferences of complex molecular species. Data were acquired over three cycles for ∼20 min. Prior the data acquisition, a 30 μm surface raster for 120 s was carried out to clean the analytical site. Zircon standard SL13 (Claoué-Long et al., 1995; Hiess et al., 2008) was used for Ti, Pb and U abundance calibrations, whereas zircon standard 91500 (Wiedenbeck et al., 2004) was used for normalization of Hf. The other trace element concentrations were determined using the relative sensitivity factors of $M^+/^{49}Ti^+$ measured from NIST SRM 610 glass (Pearce et al., 1997).

For high-precision U–Pb dating, individual zircon grains extracted from the thin sections were cleaned with 2 N HNO_3 and spiked with a mixed ^{202}Pb–^{205}Pb–^{229}Th–^{233}U–^{236}U tracer (Amelin et al., 2010). The spiked grains were digested in concentrated $HF + HNO_3$ at 220 °C, followed by evaporation and dissolution in 6 N HCl at 180 °C, in sealed metal autoclaves. The solution samples were further taken to dryness on a hotplate and brought
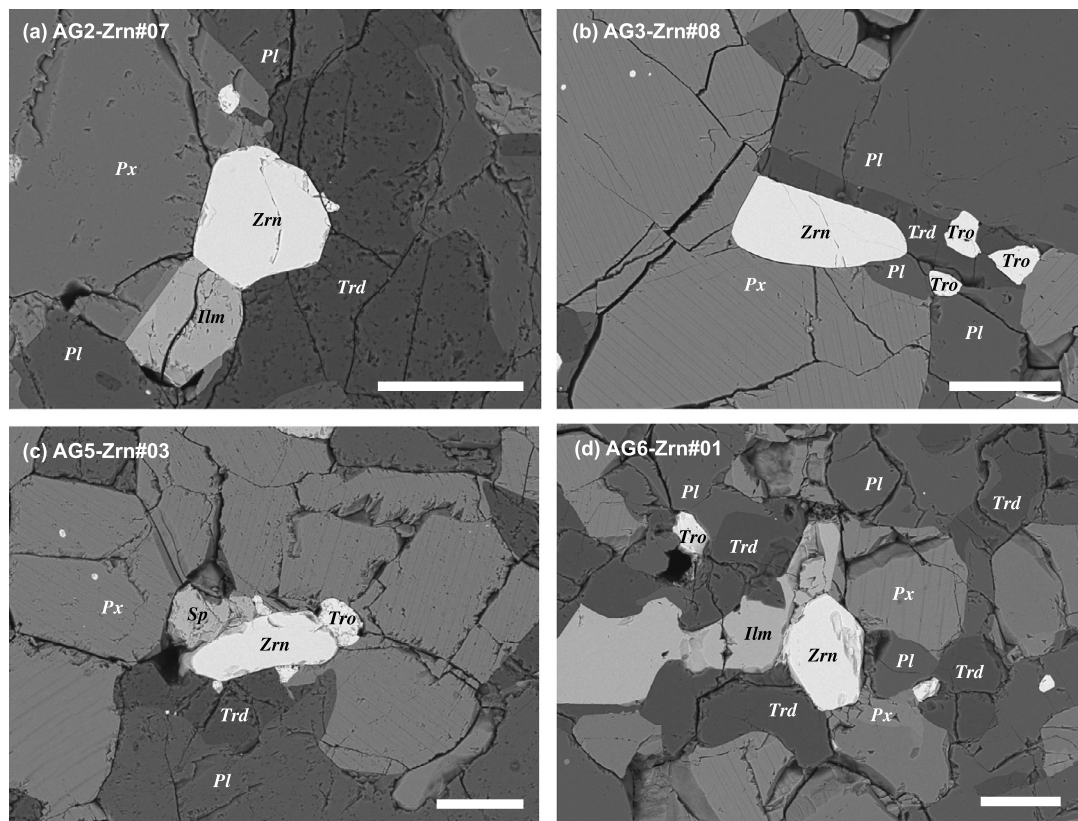
Fig. 1. Back-scattered electron images showing zircon grains (a) AG2-Zrn#07, (b) AG3-Zrn#08, (c) AG5-Zrn#03 and (d) AG6-Zrn#01 within the mesostasis of the eucrite Agoult. Scale bars are 50 µm. Mineral abbreviations are as follow: Ilm, ilmenite; Pl, plagioclase; Px, pyroxene; Sp, spinel; Trd, tridymite; Tro, troilite; Zrn, zircon.
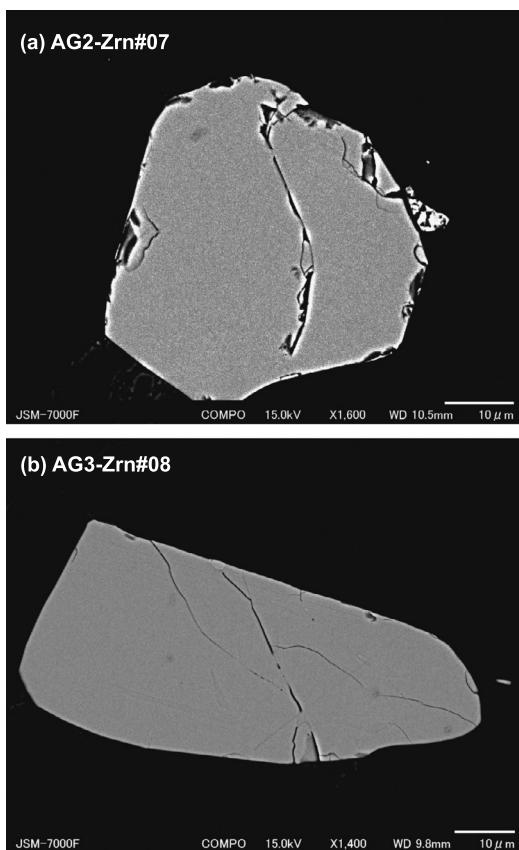
Fig. 2. Back-scattered electron images of zircon grains (a) AG2-Zrn#07 and (b) AG3-Zrn#08, showing no clear zoning structure.

back into solution in 2.5 N HCl. The separation of Pb and U was performed using columns packed with 0.05 ml of anion exchange resin AG1x8 200–400 mesh (Eichrom Technologies, U.S.A.), in which matrix elements were eluted in 2.5 N HCl followed by elution of Pb and U in 0.5 N HNO$_3$. The Pb and U isotopic measurements were performed on a Finnigan TRITON *plus* at the ANU. To enhance the emission of Pb$^+$, samples were loaded with mixtures of phosphoric acid and silicagels from Aldrich (Huyskens et al., 2012). Isotopes of Pb$^+$ and UO$_2^+$ were measured in a peak-jumping mode on the secondary electron multiplier. Instrumental mass fractionation was corrected for Pb and U based on the measured ^{202}Pb/^{205}Pb and ^{265}(UO$_2$)/^{268}(UO$_2$), respectively. Reproducibility and accuracy of U–Pb isotopic measurements during the course of this study were evaluated by analyses of an EARTHTIME synthetic 2000 Ma U–Pb standard solution spiked with the same mixed tracer as the samples (^{207}Pb/^{206}Pb age = 2000.2 ± 1.3 Ma, 2 s.d., $n = 5$).

For analyses of zircon samples, all non-radiogenic Pb was attributed to procedural blank. Five procedural blanks were independently measured using the same procedure as the zircon samples. Typical blank amounts were 2 pg for Pb and 0.01 pg for U, and the Pb isotopic ratios were ^{206}Pb/^{204}Pb = 17.798 ± 0.631, ^{207}Pb/^{204}Pb = 15.299 ± 0.616, and ^{208}Pb/^{204}Pb = 37.12 ± 1.36 (2σ). The measured blank Pb isotopic ratios were used to correct for non-radiogenic Pb in the zircon samples.

3. Results

The trace element data are summarized in Table 1. The chondrite-normalized REE abundances for single-spot analyses are plotted in Fig. 3. The Agoult zircons have Ti contents ranging from 37 to 55 ppm. The Nb contents are lower than 3 ppm, whereas Y and Hf contents are 190–420 and 5600–9500 ppm, respectively.
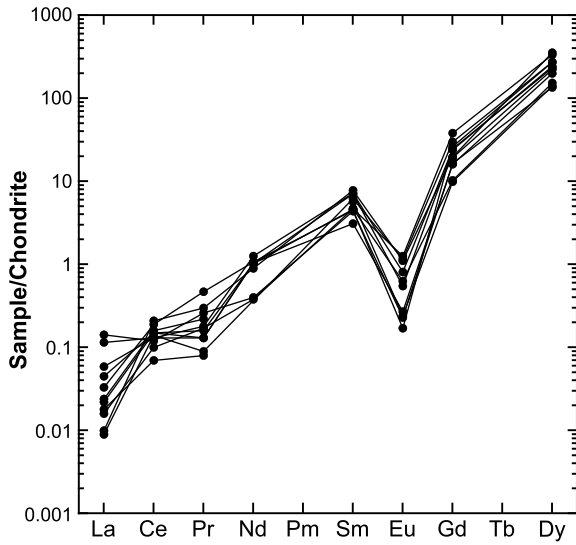
Fig. 3. Chondrite-normalized REE patterns of Agoult zircon. The chondrite data are from McDonough and Sun (1995).

All grains have REE patterns with strong depletion in LREE and prominent negative Eu anomalies (Fig. 3), like typical terrestrial zircons. Positive Ce anomalies are present, but much smaller than usually observed in terrestrial zircons. The results are consistent with previous observations for eucrite zircons (Ireland and Bukovanska, 1992; Srinivasan et al., 2007; Haba et al., 2014). To evaluate the magnitude of Ce and Eu anomalies, we calculated Ce/Ce* and Eu/Eu* where Ce* and Eu* were interpolated from chondrite-normalized abundances of the neighboring REEs assuming smooth chondrite-normalized patterns (Table 1). We obtained mean Ce/Ce* and Eu/Eu* values of 1.9 ± 1.7 (2 s.d., after rejection of one outlier) and 0.06 ± 0.06 (2 s.d.), respectively.

The U–Pb isotopic data are summarized in Table 2 and plotted on a concordia diagram in Fig. 4a. For calculations of $^{207}Pb/^{235}U$ ratios and $^{207}Pb/^{206}Pb$ dates of Agoult zircons, we used a $^{238}U/^{235}U$ value of 137.708 ± 0.016 (2σ) obtained from the Agoult whole-rock samples (Kaltenbach, 2013). The errors of $^{207}Pb/^{206}Pb$ dates are propagated to include analytical uncertainties in $^{238}U/^{235}U$ and $^{207}Pb/^{206}Pb$ ratios. The deviation of the measured $^{238}U/^{235}U$ value from the previously assumed value of 137.88 results in a -1.81 Ma change in $^{207}Pb/^{206}Pb$ date calculation, which is substantial relative to the $^{207}Pb/^{206}Pb$ age precisions (Table 2). Notably, the Agoult $^{238}U/^{235}U$ value is even lower than those of most early solar system materials, except CAIs, which yield a mean of 137.79 ± 0.02 (Amelin et al., 2010; Bouvier et al., 2011; Brennecka and Wadhwa, 2012; Connelly et al., 2012; Kaltenbach, 2013; Iizuka et al., 2014). The difference between the Agoult and meteoritic average $^{238}U/^{235}U$ values corresponds to a -0.86 Ma change in $^{207}Pb/^{206}Pb$ date calculation. All dated zircon grains have concordant U–Pb systems and identical $^{207}Pb/^{206}Pb$ dates within analytical uncertainty (Fig. 4), suggesting that U–Pb systems remain intact since the crystallization. The $^{207}Pb/^{206}Pb$ dates yield a weighted average of 4554.5 ± 2.0 Ma (2σ, MSWD = 1.05). We calculated Th/U ratios for individual grains using the ^{208}Pb abundances and $^{207}Pb/^{206}Pb$ dates, assuming the concordance between $^{207}Pb/^{206}Pb$ and $^{208}Pb/^{232}Th$ dates. All but one grains yield Th/U ratios of 0.11–0.17.

4. Discussion

4.1. Genesis and crystallization conditions of the Agoult zircon

Eucrite zircon is typically located in the mesostasis comprising ilmenite, silica minerals and troilite, and often occurs as a rim

Table 1
Trace element data for Agoult zircon.

Grain number	AG2-Zrn#05	AG2-Zrn#07	AG3-Zrn#01		AG3-Zrn#07	AG3-Zrn#08			AG3-Zrn#09	AG5-Zrn#03	
Spot number	1	1	1	2	1	1	2	3	1	1	2
Ti	41±2	42±4	44±3	43±3	37±2	55±3	46±3	46±3	37±3	52±3	40±2
Y	336±17	316±11	221±6	188±6	190±7	266±9	359±10	269±8	348±11	417±12	373±10
Nb	1.7±0.7	1.9±0.6	1.3±0.5	2.1±0.6	1.2±0.5	1.8±0.6	2.3±0.6	2.0±0.6	3.0±0.8	1.4±0.5	0.8±0.4
La	0.027±0.010	0.014±0.008	0.006±0.006	0.004±0.004	0.034±0.016	0.011±0.009	0.008±0.007	0.005±0.006	0.002±0.004	0.004±0.006	0.002±0.004
Ce	0.078±0.019	0.077±0.019	0.098±0.039	0.061±0.016	0.077±0.037	0.092±0.060	0.114±0.043	0.091±0.037	0.126±0.048	0.045±0.028	0.086±0.036
Pr	0.017±0.007	0.012±0.007	0.020±0.015	0.016±0.007	0.024±0.018	0.012±0.012	0.043±0.021	0.015±0.013	0.028±0.019	0.007±0.009	0.009±0.010
Nd	0.57±0.14	0.47±0.13	–	0.18±0.07	0.18±0.25	0.49±0.35	0.02±0.012	0.47±0.38	0.41±0.39	–	–
Sm	1.1±0.1	1.0±0.1	0.84±0.37	0.70±0.11	0.66±0.35	0.66±0.30	0.46±0.41	0.68±0.38	1.16±0.47	0.69±0.35	0.91±0.38
Eu	0.046±0.016	0.031±0.014	0.01±0.03	0.04±0.01	0.01±0.03	0.01±0.02	0.02±0.29	–	0.06±0.06	0.07±0.06	0.07±0.06
Gd	4.9±0.8	4.8±0.8	2.0±0.7	2.1±0.5	3.3±1.0	5.2±1.5	3.2±0.03	3.8±1.1	3.9±1.5	7.6±1.5	6.0±1.2
Dy	57±14	60±13	35±6	38±13	33±33	67±10	49±1.4	55±16	87±10	82±15	68±16
Hf	8621±600	8994±655	7014±470	8165±547	7633±533	9473±652	5609±379	8287±561	9556±651	6884±465	6919±464
Pb	92±7	101±7	62±5	66±5	70±7	88±6	75±5	71±5	95±6	80±14	88±6
U	63±5	67±5	44±4	49±4	48±5	61±5	50±4	52±4	71±5	68±16	61±5
Ti-temp (°C)[a]	897±23	902±28	908±22	904±25	885±23	935±23	912±22	913±23	886±26	928±23	895±22
Ce/Ce*[a]	0.9±0.3	1.4±0.6	2.2±1.7	1.9±1.1	0.7±0.4	2.0±1.9	1.5±0.9	2.5±2.0	3.7±3.8	2.0±2.2	4.9±5.6
Eu/Eu*	0.061±0.023	0.043±0.020	0.032±0.063	0.090±0.037	0.027±0.057	0.039±0.077	0.016±0.033	–	0.090±0.092	0.094±0.088	0.086±0.078

Notes: All concentrations are presented in ppm. All errors are reported at the 68% confidence level.
[a] Temperatures calculated using calibration of Ferry and Watson (2007) under the assumption that SiO_2 and TiO_2 activities are 1.

Table 2
U–Pb isotopic data for Agoult zircon grains.

Grain	U (pg)	Pb (pg)	Isotopic ratios[a]									Dates (Ma)						%disc[d]	Th/U model ratio[e]
			206Pb/204Pb[b]	208Pb/206Pb	207Pb/235U	%error	206Pb/238U	%error	207Pb/206Pb	%error	Error corr.[c] 6/8–7/5	206Pb/238U	Error	207Pb/235U	Error	207Pb/206Pb	Error		
AG2-Zrn#02	1.8	4.5	82	0.032	88.060	3.74	1.0288	5.09	0.6216	1.53	0.986	4560	121	4558	50	4557.5	22.2	−0.1	0.13
AG2-Zrn#07	10.6	18.3	262	0.028	88.042	0.99	1.0292	1.35	0.6212	0.44	0.978	4562	32	4558	13	4556.6	6.4	−0.2	0.11
AG3-Zrn#07	3.0	5.9	123	0.004	86.373	2.44	1.0100	3.24	0.6210	0.97	0.982	4500	79	4539	32	4556.2	14.0	1.7	0.02
AG3-Zrn#08	4.5	10.3	97	0.041	88.047	2.97	1.0269	4.09	0.6226	1.25	0.987	4555	96	4558	40	4559.9	18.1	0.2	0.17
AG3-Zrn#09	13.9	22.3	443	0.029	87.538	0.73	1.0239	0.91	0.6209	0.29	0.962	4545	24	4552	9	4555.8	4.2	0.3	0.12
AG4-Zrn#10	2.0	4.5	103	0.032	87.717	3.19	1.0279	4.13	0.6197	1.17	0.981	4558	103	4554	41	4553.0	17.0	−0.1	0.13
AG5-Zrn#03	18.3	29.0	503	0.030	87.468	0.59	1.0223	0.76	0.6213	0.27	0.957	4540	19	4552	8	4556.9	3.8	0.5	0.12
AG6-Zrn#01	17.8	27.8	619	0.034	87.447	0.48	1.0263	0.64	0.6187	0.24	0.944	4553	16	4551	6	4550.8	3.5	−0.1	0.14

Note: All errors are reported at the 95% confidence level.
[a] Isotopic ratios corrected for blank, spike contribution, mass fractionation, and non-radiogenic Pb. All non-radiogenic Pb was assumed to be procedural blank.
[b] $^{206}Pb/^{204}Pb$ are corrected only for spike contribution and mass fractionation.
[c] Error correlation between $^{206}Pb/^{238}U$ and $^{207}Pb/^{235}U$.
[d] % discordance calculated as $100 \times (1 - [^{206}Pb/^{238}U]_{measured}/[^{206}Pb/^{238}U]_{@207Pb^*/206Pb^* date})$.
[e] Model Th/U ratio estimated from ^{208}Pb abundance and $^{207}Pb/^{206}Pb$ date.
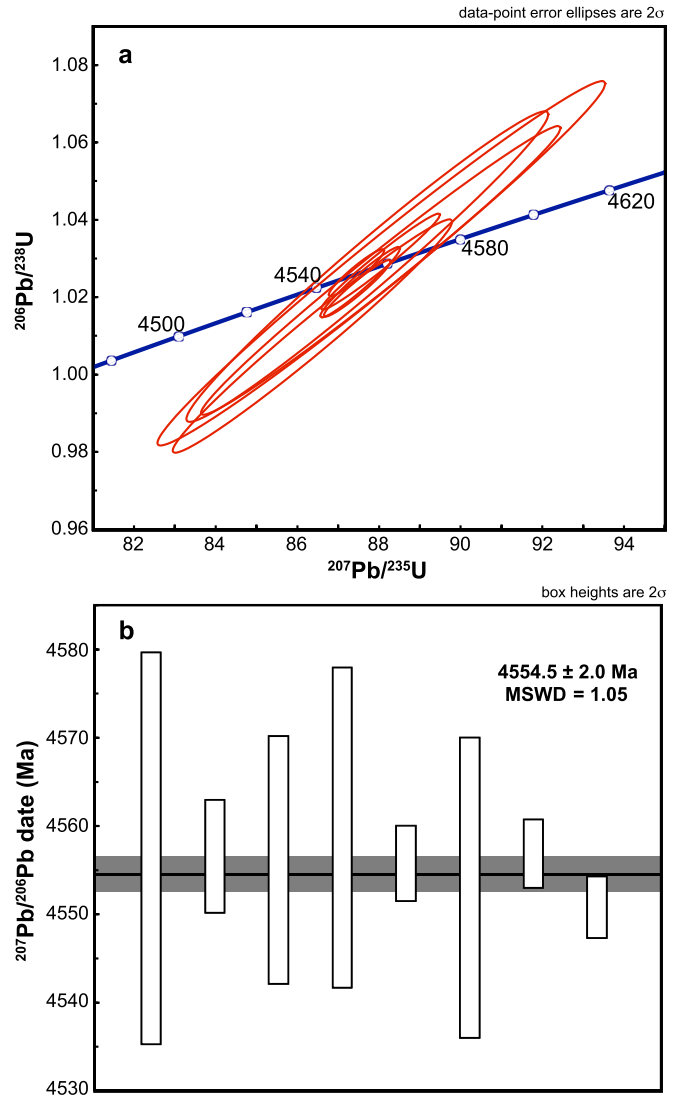
Fig. 4. U–Pb isotopic data for zircon grains from the eucrite Agoult. (a) Wetherill concordia diagram. (b) $^{207}Pb/^{206}Pb$ dates and the weighted average (bold line) with 95% confidence interval (shaded area). Errors at 95% confidence level are represented by (a) ellipses and (b) boxes, respectively. The concordia line and $^{207}Pb/^{206}Pb$ dates are calculated using $^{238}U/^{235}U = 137.708 \pm 0.016$ as determined for whole-rock fractions of Agoult (Kaltenbach, 2013).

and inclusion of ilmenite (Misawa et al., 2005; Haba et al., 2014; Roszjar et al., 2014). The zircon grain size and shape vary from sample to sample as well as within individual samples, but the grains tend to be large and euhedral in highly metamorphosed eucrites such as A-881388 and A-881467 (Haba et al., 2014). These observations, in conjunction with the zircon REE pattern inconsistent with its crystallization from a residual melt of plagioclase and pyroxene fractional crystallization, led Haba et al. (2014) to suggest the significance of metamorphic zircon growth in eucrites. As mentioned in Section 2, Agoult has granulitic textures indicative of strong recrystallization during high-temperature metamorphism (Yamaguchi et al., 2009). Thus, our finding of large (∼80 µm) zircon grains with euhedral to subhedral shapes in Agoult follows the noted trend between the eucrite zircon morphology and metamorphic grade.

The occurrence of zircon rim and corona around ilmenite has been observed also in terrestrial mafic plutonic and granulite-facies metamorphic rocks (e.g., Bingen et al., 2001; Söderlund and Söderlund, 2004; Morisset and Scoates, 2008). Considering that baddeleyite as well as Cr-spinel occurs as an exsolution phase of ilmenite

(Naslund, 1987), the close association of ilmenite and zircon has been interpreted to reflect zircon formation by Zr release from ilmenite followed by its reaction with silica during slow magmatic cooling and granulite-facies metamorphism (Bingen et al., 2001; Charlier et al., 2007). This interpretation is supported by the results of combined Ti-in-zircon and Zr-in-rutile thermometry of terrestrial granulite-facies metamorphic rocks (Baldwin and Brown, 2008; Ewing et al., 2013): co-existing rutile and zircon grains as well as zircon grains associated with ilmenite record substantially lower temperatures than the peak metamorphic temperatures (i.e., low Zr-in-rutile and Ti-in-zircon contents), whereas analyses of mixtures of tiny exsolved Zr phases (baddeleyite or zircon) and their host rutile grains yielded high Zr contents corresponding to the peak metamorphic temperatures. These results indicate zircon growth by Zr release from rutile and ilmenite during slow cooling from the metamorphic thermal maximum.

The application of Ti-in-zircon thermometry can be extended to extra-terrestrial zircon by taking into account the effects of SiO_2 and TiO_2 activity (a_{SiO_2} and a_{TiO_2}) and pressure (Valley et al., 2014). At pressures around 1 GPa, the equilibrium Ti-in-zircon content is expressed by (Ferry and Watson, 2007):

$$\log(\text{Ti-in-zircon [ppm]}) = (5.711 \pm 0.072) - (4800 \pm 86)/T \text{ [K]}$$
$$- \log a_{SiO_2} + \log a_{TiO_2} \qquad (1)$$

The presence of tridymite and ilmenite in Agoult indicates $a_{SiO_2} = 1$ and $a_{TiO_2} < 1$. While a_{TiO_2} in crustal rocks are generally 0.6 or higher (Hayden and Watson, 2007), use of $a_{TiO_2} = 0.6$–0.74 obtained from metabasic and gabbroic rocks (Ghent and Stout, 1984; Ickert et al., 2011) would increase temperatures by 40–70 °C relative to $a_{TiO_2} = 1$. On the other hand, low pressure conditions in Vesta's crust would require corrections of −50 to −100 °C as compared to the estimates at ca. 1 GPa (Ferry and Watson, 2007; Ferriss et al., 2008). Accordingly, the corrections for a_{TiO_2} and pressure largely cancel each other out. We therefore estimated approximate temperatures of Agoult zircon crystallization using Eq. (1) assuming $a_{SiO_2} = a_{TiO_2} = 1$.

The Ti contents of 37–55 ppm in the Agoult zircon grains yield crystallization temperatures of 885–935 °C with the average of 905 ± 32 °C (2 s.d.) (Table 2). The estimated temperatures are substantially lower than the eutectic point of eucrite at ca. 1050 °C (Stolper, 1977; Yamaguchi et al., 2013) and are similar to the equilibration temperatures of pyroxenes in basaltic eucrites (Yamaguchi et al., 1996). Considering that the relict subophitic texture of Agoult requires its rapid igneous crystallization, such subsolidus zircon formation would occur not during the igneous crystallization but during prolonged high-temperature metamorphism. The relatively low Th/U ratios in the Agoult zircon (0.11–0.17) compared to typical terrestrial igneous zircons (0.4–1.0, Hoskin and Ireland, 2000) support the metamorphic zircon formation, possibly by Zr release from ilmenite. Indeed, some ilmenite grains in Agoult do contain tiny needles or blobs of baddeleyite and spinel (Fig. 5), indicating exsolution of these phases from ilmenite. Furthermore, we find that the ilmenite grains show a significant variation in Zr and Hf contents with nearly constant Nb and Ta contents (Fig. 5 and Supplementary Table), suggesting significant Zr migration within the ilmenite grains. The Zr exsolution and migration could proceed more efficiently at a higher metamorphic temperature, resulting in formation of relatively large zircon grains in highly metamorphosed eucrites.

For a zircon with known crystallization temperature, the magnitude of Ce anomaly in the zircon can be used to constrain the oxygen fugacity (fO_2) during the crystallization (Trail et al., 2011, 2012). The Ce/Ce* value of 1.9 ± 1.7 (2 s.d.) combined with the crystallization temperature of 905 ± 32 °C (2 s.d.) for the Agoult zircon constrains the fO_2 to below that of the iron–wüstite (IW)
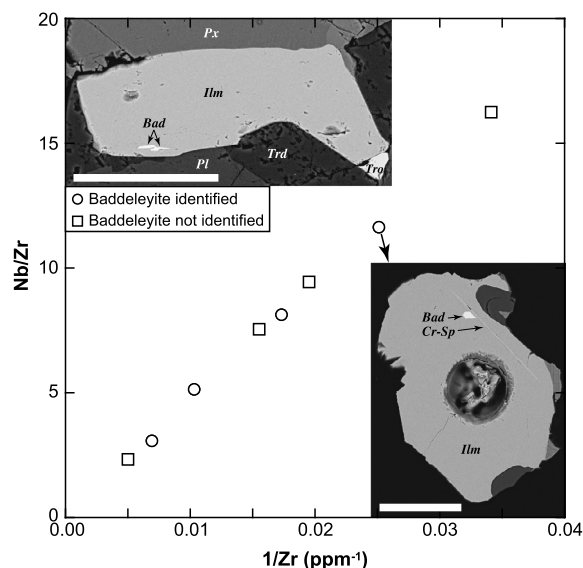

Fig. 5. Plot of 1/Zr versus Nb/Zr for ilmenite grains in the Agoult eucrite, some of which are identified as including baddeleyite (Bad). Inset pictures show backscattered electron images of the ilmenite grains associated with baddeleyite as well as chromite. Mineral abbreviations are the same as those used in Fig. 1.
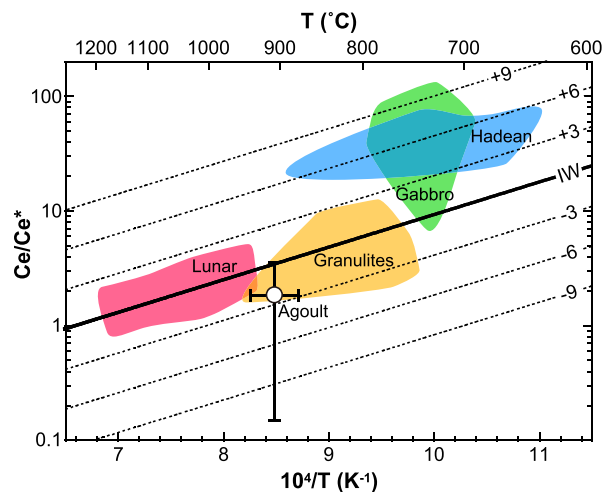

Fig. 6. Plot of Ce/Ce* versus $1/T$ for Agoult zircon, with experimentally calibrated oxygen fugacity curves relative to the iron–wüstite (IW) buffer (after Trail et al., 2011). Shaded areas show the fields of lunar zircons (Taylor et al., 2009) and terrestrial zircons (Hadean detrital zircons with $\delta^{18}O$ in the mantle equilibrium range, Cavosie et al., 2005, 2006; Fu et al., 2008; magmatic zircons from a gabbro with $\delta^{18}O$ in the mantle equilibrium range, Fu et al., 2009, metamorphic zircons from granulites, Ewing et al., 2013). The Agoult zircon data indicate its crystallization at an fO_2 below than the IW buffer.

buffer (Fig. 6). This is more reducing than crystallization conditions of terrestrial zircons with mantle-like O isotopic signatures (Cavosie et al., 2005, 2006; Fu et al., 2008, 2009) but similar to those of lunar zircons (Trail et al., 2011 after Taylor et al., 2009) as well as terrestrial metamorphic zircons associated with ilmenite in highly reduced granulites (Harlov and Förster, 2002; Ewing et al., 2013). Furthermore, the estimated fO_2 is consistent with the close association of ulvöspinel–ilmenite–troilite in Agoult, which is suggestive of fO_2 conditions between IW and iron–ilmenite–ulvöspinel buffers (El Goresy and Ramdohr, 1975; Shearer et al., 2012). Overall, mineralogical and geochemical evidence indicate that the Agoult zircon formed at ca. 900 °C and fO_2 below that of the IW buffer via Zr release from ilmenite during prolonged thermal metamorphism.
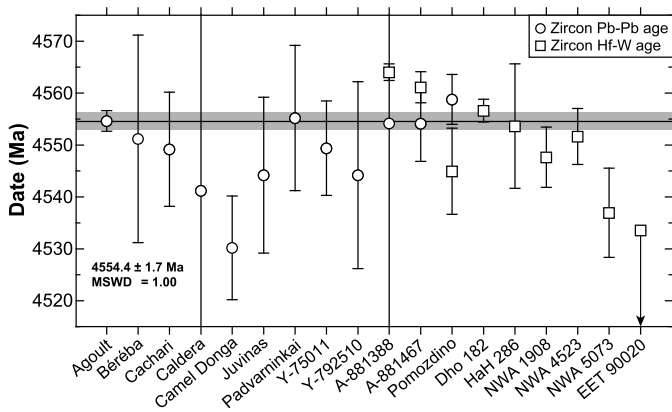
Fig. 7. Comparison of zircon Pb–Pb and Hf–W dates for basaltic eucrites. The black solid line with gray shaded area show the weighted mean and 95% confidence interval of zircon Pb–Pb dates of all basaltic eucrites except Camel Donga. Error bars on individual points show the weighted errors at 95% confidence level. Data sources are as follow: Agoult, this study; Pb–Pb dates of Béréba, Cachari, Caldera, Camel Donga and Juvinas, Zhou et al. (2013); Pb–Pb dates of Asuka (A)-881388, Padvarninkai, Yamato (Y)-75011 and Y-792510, Misawa et al. (2005); Pb–Pb date of A-881467, Misawa et al. (2005) and Srinivasan et al. (2004); Pb–Pb and Hf–W dates of Pomozdino, Ireland and Bukovanska (2003); Hf–W dates of A-881388, A-881467 and Elephant Moraine (EET) 90020, Srinivasan et al. (2007); Hf–W dates of Dhofar (Dho) 182, Hammadah al Hamra (HaH) 286, Northwest Africa (NWA) 1908, NWA 4523 and NWA 5073, Roszjar et al. (2012). Note that all previously reported zircon Pb–Pb dates were recalculated using the $^{238}U/^{235}U$ value of 137.79 ± 0.02, an approximate estimate for most solar system materials except CAIs (Amelin et al., 2010; Bouvier et al., 2011; Brennecka and Wadhwa, 2012; Connelly et al., 2012; Kaltenbach, 2013; Iizuka et al., 2014), and that all Hf–W dates were recalculated against Hf–W isotopic data of Kleine et al. (2012) for D'Orbigny.

4.2. The crystallization age of eucrite zircon

All analyzed Agoult zircon grains have identical $^{207}Pb/^{206}Pb$ dates with concordant U–Pb systems (Fig. 4), validating that the U–Pb systems are pristine since the crystallization and, therefore, that the weighted average value of the $^{207}Pb/^{206}Pb$ dates, 4554.5 ± 2.0 Ma (2σ, MSWD = 1.05), can be interpreted to reflect the time of the zircon crystallization. In Fig. 7, we compare the Agoult zircon $^{207}Pb/^{206}Pb$ age with previously reported zircon $^{207}Pb/^{206}Pb$ and Hf–W dates for basaltic eucrites. All Hf–W dates were recalculated relative to an initial $^{182}Hf/^{180}Hf$ of $(7.15 \pm 0.17) \times 10^{-5}$ (Kleine et al., 2012) at 4563.37 ± 0.25 Ma ($^{207}Pb/^{206}Pb$ age, Brennecka and Wadhwa, 2012 after Amelin, 2008) for D'Orbigny. All but one (Camel Donga) previously reported zircon $^{207}Pb/^{206}Pb$ dates are identical within uncertainties ($\pm \geq 5$ Ma) and yield the weighted value of 4554.1 ± 3.1 Ma (2σ, MSWD = 0.99), in excellent agreement with the Agoult zircon $^{207}Pb/^{206}Pb$ age. Including the Agoult zircon $^{207}Pb/^{206}Pb$ age in the weighted average calculation results in the value of 4554.4 ± 1.7 Ma (2σ, MSWD = 0.90). The chronological correspondence indicates either ubiquitous zircon growth or significant U–Pb age resetting in pre-existing zircon at 4554 Ma. We envisage that the latter process would be relatively minor, however, because at estimated cooling rates of $\geq 4000\,°C/Ma$ for thermal metamorphism of basaltic eucrites (Miyamoto and Takeda, 1977; Schwartz and McCallum, 2005) Pb closure temperatures for zircon with an effective radius of 20 µm would be higher than the solidus temperature (i.e., $\geq 1060\,°C$, after Cherniak and Watson, 2003). Such high temperature metamorphic conditions are unlikely for most of the basaltic eucrites showing no evidence of partial melting. The distinctly younger Camel Donga zircons (4530 ± 10 Ma, Zhou et al., 2013) could have formed during a later metamorphic event through breakdown of a FeO-bearing phase containing substantial amounts of Zr, considering that this meteorite is unique in its high metal content probably due to reduction of FeO and FeS by S_2 and SO_2 loss during short-term annealing event (Palme et al., 1988). The younger zircon $^{207}Pb/^{206}Pb$

age of Camel Donga is identical to the $^{207}Pb/^{206}Pb$ age of Agoult plagioclase (Iizuka et al., 2013), suggesting that the short-term annealing event is recorded not by Agoult zircon but by Agoult plagioclase.

The eucrite zircon ($\pm$pyroxene) Hf–W isochron dates are generally consistent with the eucrite zircon $^{207}Pb/^{206}Pb$ ages of either 4555 Ma or 4530 Ma. In detail, however, A-881388 and A-881467 gave zircon-pyroxene Hf–W isochron dates (4564.0 ± 1.6 and, 4561.1 ± 3.0 Ma, after Srinivasan et al., 2007) distinctly older than the weighted average of the zircon $^{207}Pb/^{206}Pb$ ages. The discrepancy may be attributed to preferential resetting of the U–Pb system over the Hf–W system in igneous zircon during thermal metamorphism at 4554 Ma, since diffusion of Pb in zircon is faster than those of Hf and W (Cherniak and Watson, 2003). Alternatively, the older Hf–W dates may reflect inheritance of radiogenic W in metamorphic zircon from igneous zircon/baddeleyite. Zircon can incorporate non-trivial amounts of W during the crystallization especially under reducing conditions where W is largely present as W^{4+}. The substantial W incorporation is manifested by the only moderately high ratios of radiogenic ^{182}W to initial ^{182}W in eucrite zircon ($\sim$10). Thus, if the igneous precursors of the metamorphic zircon grains in the A-881388 and A-881467 were zircon and/or baddeleyite having significantly high Hf/W, then the inheritance of highly radiogenic W would result in the apparent old Hf–W date for the metamorphic zircon grains.

4.3. Constraints on the thermal history of basaltic crust on Vesta

On the basis of mineralogy and chemistry of basaltic eucrites, basaltic crust on Vesta has been considered to experience at least the following thermal events (Takeda and Graham, 1991; Metzler et al., 1995; Yamaguchi et al., 1996, 2001, 2009; Bogard and Garrison, 2003; Treiman et al., 2004; Barrat et al., 2011; Warren et al., 2014): (a) rapid igneous crystallization to produce subophitic textures, (b) a prolonged global metamorphism with temperatures ranging from $\sim$800 to 1000 °C that resulted in homogenization and exsolution of pyroxene in most eucrites and strong recrystallization in granulitic eucrites (e.g., Agoult, A-881388 and A-881467), which is followed by (c) an instantaneous heating event with a peak temperature up to the solidus temperature (ca. 1050 °C, Stolper, 1977; Yamaguchi et al., 2013) that lead to partial melting of several eucrites and to form high-temperature phases such as tridymite and Ti-rich spinel (e.g., Agoult and EET 90020), (d) impact events that caused brecciation accompanied by short-term heating and rapid cooling, (e) a metasomatism possibly by fluids to form veins consisting mainly of Fe-rich olivine in several eucrites (e.g., Yamato (Y)-75011 and Northwest Africa (NWA) 5738). The instantaneous heating event (c) may be identical to the impact event (d).

To set chronological constraints on these thermal events, basaltic eucrites have been dated with several isotopic chronometers. The reported dates are highly variable, but it is generally accepted that the earliest eucrite crystallization took place within the first few million years of the solar system as indicated by the oldest inter-mineral Mn–Cr and Al–Mg isochron dates (Lugmair and Shukolyukov, 1998; Srinivasan et al., 1999) and that younger Ar–Ar dates of 4.1–3.5 Ga represent Ar degassing by impact events (Kunz et al., 1995; Bogard and Garrison, 2003). Yet geologic significance of the most common isotopic dates between 4.56 and 4.4 Ga (e.g., $^{207}Pb/^{206}Pb$, Manhes et al., 1984; Tera et al., 1997; Iizuka et al., 2013; Sm–Nd, Nyquist et al., 1997; Boyet et al., 2010; Mn–Cr, Lugmair and Shukolyukov, 1998; Hf–W, Kleine et al., 2005; Pu–Xe, Shukolyukov and Begemann, 1996) are still controversial. A major difficulty in interpreting the geologic significance is that the isochron dates were defined using multiple minerals which show different behavior during post-crystallization
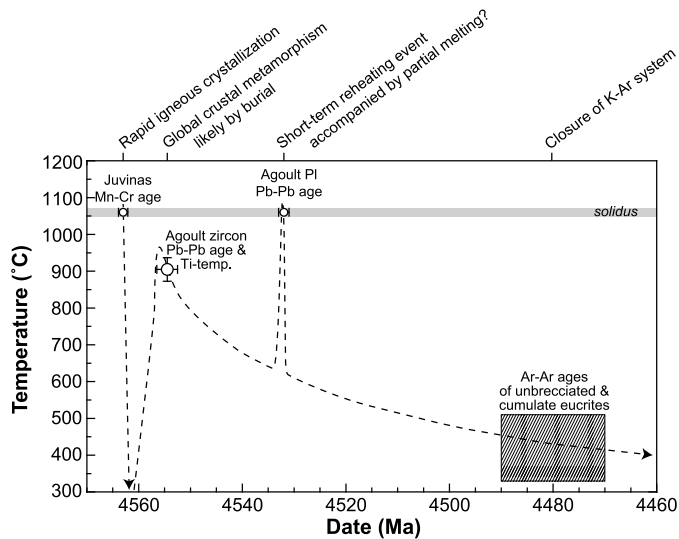
Fig. 8. Thermal history of highly metamorphosed basaltic eucrites. Gray band shows the solidus temperature of eucrites (Stolper, 1977; Yamaguchi et al., 2013). The crystallization age of basaltic eucrite is taken from the inter-mineral isochron Mn–Cr date of Juvinas (after Lugmair and Shukolyukov, 1998). The Pb–Pb age of Agoult plagioclase is from Iizuka et al. (2013). The Ar–Ar dates of unbrecciated and cumulate eucrites are from Bogard and Garrison (2003), which may reflect closure of K–Ar system in relatively deep Vesta's crust. The closure temperatures of the K–Ar system was estimated using the Ar diffusion parameters in plagioclase of Cassata et al. (2009) with cooling rates between 4000 and 350 000 K/Ma (Miyamoto and Takeda, 1977, 1994).

thermal events and, in some cases, whose diffusion rates are poorly constrained. This difficulty can be circumvented by applying zircon U–Pb chronology because single coarse grains of zircon can be precisely dated by the U–Pb method and the isotopic data can validate whether it remained a closed U–Pb system. Furthermore, the combination of high-precision U–Pb dating and Ti-thermometry on zircon allows us to unambiguously link the zircon U–Pb age with a certain geologic event.

In some of the previous studies (Misawa et al., 2005; Zhou et al., 2013), the ^{207}Pb/^{206}Pb ages of eucrite zircon have been interpreted as reflecting igneous crystallization, on the basis of high closure temperatures for Pb diffusion in zircon. However, several lines of evidence discussed above (Section 4.1) indicate that Agoult zircon formed at subsolidus temperatures of ca. 900 °C through Zr release from ilmenite during protracted thermal metamorphism, which are similar to the conditions of the pyroxene homogenization and exsolution. In addition, most eucrites yield identical zircon ^{207}Pb/^{206}Pb dates to Agoult zircon within uncertainty. Thus, we interpret the weighted average of the zircon ^{207}Pb/^{206}Pb dates (4554.4 ± 1.7 Ma, 2σ) as the timing of the metamorphic zircon growth and pyroxene exsolution during the prolonged widespread crustal metamorphism on Vesta, namely the thermal event (b) (Fig. 8). This interpretation can reconcile the discrepancy between the zircon ^{207}Pb/^{206}Pb age (4544 ± 15 Ma, after Zhou et al., 2013) and inter-mineral Mn–Cr isochron age [4563.0 ± 0.9 Ma, calculated from the Mn–Cr data of Lugmair and Shukolyukov (1998) relative to the Mn–Cr data of Glavin et al. (2004)] of the basaltic eucrite Juvinas, the latter of which is considered as the timing of the igneous crystallization. Early silicate differentiation on Vesta within the first few million years of the solar system is further indicated by whole-rock Mn–Cr and Al–Mg isochrons defined by HED meteorites (Trinquier et al., 2008; Schiller et al., 2010). The younger ^{207}Pb/^{206}Pb date of ca. 4530 Ma for Agoult plagioclase (Iizuka et al., 2013) as well as Camel Donga zircon (Zhou et al., 2013) might reflect the age of the subsequent short-term thermal event (c) causing partial melting of Agoult, given that U–Pb system of the plagioclase was preferentially re-

set during the thermal event and also that the high metal content in Camel Donga results from reduction of FeO and FeS by S_2 and SO_2 loss during short-term annealing event (Palme et al., 1988).

There are two contrasting models to explain the global metamorphism in basaltic crust on Vesta. The first is that ordinary equilibrated eucrites were produced by meteoroid impact at or near the floor/wall of a crater (Nyquist et al., 1986). The second model argues that basaltic eucrites that rapidly crystallized at or near the surface were buried under successive lava flows and metamorphosed by heating from the hot interior (Yamaguchi et al., 1996, 2001, 2009). Notably, the thermal metamorphic age as constrained by Agoult zircon is coincident with the oldest, and probably igneous, age of cumulate eucrites (Mn–Cr age of 4553.8 ± 2.5 Ma for Serra de Magé, Lugmair and Shukolyukov, 1998). In addition, non-brecciated but highly metamorphosed basaltic eucrites and cumulate eucrites have Ar–Ar ages of ca. 4.48 Ga, which are significantly older than those between 4.1 and 3.5 Ga for brecciated basaltic eucrites (Yamaguchi et al., 2001; Bogard and Garrison, 2003). These chronological relationships can be best explained if highly metamorphosed basaltic eucrites were located in relatively deeper part of basaltic crust where significant heat was introduced by the emplacement of cumulate eucrites and these deep crustal rocks were undisturbed by later impact events that lead to brecciation and Ar-degassing of the shallower crust, thereby supporting the model of burial crustal metamorphism.

The basaltic magmatism on Vesta is considered to proceed at an fO_2 of one log unit below the IW buffer based on the liquidus mineral assemblages and major element compositions of basaltic eucrites (Stolper, 1977; Jurewicz et al., 1993). On the other hand, analyses of Cr-spinels in fluid-metasomatic veins in the eucrite NWA 5738 indicate the vein formation at an fO_2 of three log unit above the IW buffer (Warren et al., 2014). The new constraint on the fO_2 during Agoult zircon crystallization (Fig. 5) suggests that basaltic crust had remained under reducing conditions during the high-temperature metamorphism at 4554 Ma. This is in striking contrast with oxidation of the ordinary chondrites during thermal metamorphism possibly by interaction with an oxidizing vapor phase such as H_2O (McSween and Labotka, 1993). The implication is that although the presence of secondary Fe-rich olivine and quartz veins in some eucrites suggests a metasomatism accompanied by oxidation by aqueous fluid in Vesta's crust (Treiman et al., 2004; Barrat et al., 2011; Warren et al., 2014), such oxidizing phase was absent within the Agoult crust at least until 4554 Ma.

5. Conclusions

The Agoult eucrite having granulitic textures contains large zircon grains with sizes up to 80 μm, allowing us to conduct the first combined high-precision U–Pb isotopic and trace element analyses on eucrite zircon. All eight U–Pb isotopic analyses plot on concordia line and provide consistent ^{207}Pb/^{206}Pb ages with the weighted average of 4554.5 ± 2.0 Ma (2σ). The zircon ^{207}Pb/^{206}Pb age is in good agreement with previously reported but less precise zircon ^{207}Pb/^{206}Pb ages for most basaltic eucrites, suggesting ubiquitous zircon growth in basaltic crust on Vesta at that time. The Ti contents in Agoult zircon indicate the crystallization temperatures of ca. 900 °C, which are similar to the subsolidus equilibration temperatures of pyroxenes from most basaltic eucrites (Yamaguchi et al., 1996). The crystallization temperatures, together with the presence of baddeleyite needles in ilmenite and various Zr-in-ilmenite contents, indicate that Agoult zircon formed by Zr release from ilmenite followed by reaction with silica during protracted thermal metamorphism. Thus, we interpret the zircon ^{207}Pb/^{206}Pb age as the timing of the global crustal metamorphism on Vesta that lead to homogenization and exsolution of pyroxene in most

basaltic eucrites. The REE patterns of the Agoult zircon grains display restricted positive Ce anomalies, like zircon grains from other eucrites (Ireland and Bukovanska, 1992; Srinivasan et al., 2007; Haba et al., 2014). Combining the magnitude of Ce anomaly with the Ti-in-zircon crystallization temperature, fO_2 during the zircon crystallization is constrained to below that of IW buffer, which is similar to the estimated fO_2 for eucrite igneous crystallization (Stolper, 1977; Jurewicz et al., 1993). This suggests that an oxidizing agent such as H_2O was absent within the crust at 4554 Ma.

Acknowledgements

Appendix A. Supplementary material

Supplementary material related to this article can be found online at http://dx.doi.org/10.1016/j.epsl.2014.10.055.

References

Amelin, Y., 2008. U–Pb ages of angrites. Geochim. Cosmochim. Acta 72, 221–232.

Amelin, Y., Kaltenbach, A., Iizuka, T., Stirling, C.H., Ireland, T.R., Petaev, M., Jacobsen, S.B., 2010. U–Pb chronology of the Solar System's oldest solids with variable $^{238}U/^{235}U$. Earth Planet. Sci. Lett. 300, 343–350.

Baldwin, J.A., Brown, M., 2008. Age and duration of ultrahigh-temperature metamorphism in the Anápolis–Itauçu Complex, Southern Brasília Belt, central Brazil — constraints from U–Pb geochronology, mineral rare earth element chemistry and trace element thermometry. J. Metamorph. Geol. 26, 213–233.

Barrat, J.A., Jambon, A., Bohn, M., Blichert-Toft, J., Sautter, V., Göpel, C., Gillet, Ph., Boudouma, O., Keller, F., 2003. Petrology and geochemistry of the unbrecciated achondrite Northwest Africa 1240 (NWA 1240): an HED parent body impact belt. Geochim. Cosmochim. Acta 67, 3959–3970.

Barrat, J.A., Yamaguchi, A., Bunch, T.E., Bohn, M., Bollinger, C., Ceuleneer, G., 2011. Possible fluid–rock interactions on differentiated asteroids recorded in eucritic meteorites. Geochim. Cosmochim. Acta 75, 3839–3852.

Bingen, B., Austrheim, H., Whitehouse, M., 2001. Ilmenite as a source for zirconium during high-grade metamorphism? Textural evidence from the Caledonides of western Norway and implications for zircon geochronology. J. Petrol. 42, 355–375.

Binzel, R.P., Xu, S., 1993. Chips off of asteroid 4 Vesta: evidence for the parent body of basaltic achondrite meteorites. Science 260, 186–191.

Bogard, D.D., Garrison, D.H., 2003. $^{39}Ar–^{40}Ar$ ages of eucrites and thermal history of asteroid 4 Vesta. Meteorit. Planet. Sci. 38, 669–710.

Bouvier, A., Spivak-Birndorf, L.J., Brennecka, G.A., Wadhwa, M., 2011. New constraints on early Solar System chronology from Al–Mg and U–Pb isotope systematics in the unique basaltic achondrite Northwest Africa 2976. Geochim. Cosmochim. Acta 75, 5310–5323.

Boyet, M., Carlson, R.W., Horan, M., 2010. Old Sm–Nd ages for cumulate eucrites and redetermination of the solar system initial $^{146}Sm/^{144}Sm$ ratio. Earth Planet. Sci. Lett. 291, 172–181.

Brennecka, G.A., Wadhwa, M., 2012. Uranium isotope compositions of the basaltic angrite meteorites and the chronological implications for the early solar system. Proc. Natl. Acad. Sci. USA 109, 9299–9303.

Burbine, T.H., Buchanan, P.C., Binzel, R.P., Bus, S.J., Hiroi, T., Hinrichs, J.L., Meibom, A., McCoy, T.J., 2001. Vesta, Vestoids, and the howardite, eucrite, diogenite group: relationships and the origin of spectral differences. Meteorit. Planet. Sci. 36, 761–781.

Burnham, A.D., Berry, A.J., 2012. An experimental study of trace element partitioning between zircon and melts as a function of oxygen fugacity. Geochim. Cosmochim. Acta 95, 196–212.

Cassata, W.S., Renne, P.R., Shuster, D.L., 2009. Argon diffusion in plagioclase and implications for thermochronometry: a case study from the Bushveld Complex, South Africa. Geochim. Cosmochim. Acta 73, 6600–6612.

Cavosie, A.J., Valley, J.W., Wilde, S.A., EIMF, 2005. Magmatic $\delta^{18}O$ in 4400–3900 Ma detrital zircons: a record of the alteration and recycling of crust in the Early Archean. Earth Planet. Sci. Lett. 235, 663–681.

Cavosie, A.J., Valley, J.W., Wilde, S.A., EIMF, 2006. Correlated microanalysis of zircon: trace element, $\delta^{18}O$, and U–Th–Pb isotopic constraints on the igneous origin of complex >3900 Ma detrital grains. Geochim. Cosmochim. Acta 70, 5601–5616.

Charlier, B., Skar, O., Korneliussen, A., Duchesne, J.-C., Vander Auwera, J., 2007. Ilmenite composition in the Tellnes Fe–Ti deposit, SW Norway: fractional crystallization, postcumulus evolution and ilmenite-zircon relation. Contrib. Mineral. Petrol. 154, 119–134.

Cherniak, D.J., Watson, E.B., 2003. Diffusion in zircon. Rev. Mineral. Geochem. 53, 113–143.

Claoué-Long, J.C., Compston, W., Roberts, J., Fanning, C.M., 1995. Two carboniferous ages: a comparison of SHRIMP zircon dating with conventional zircon ages and $^{40}Ar/^{39}Ar$ analysis. In: Berggren, W.A., Kent, D.V., Aubry, M.P., Hardenbol, J. (Eds.), Geochronology, Time Scales and Global Stratigraphic Correlation, vol. 54. SEPM Special Publication, pp. 3–21.

Clayton, R.N., Onuma, N., Mayeda, T.K., 1976. A classification of meteorites based on oxygen isotopes. Earth Planet. Sci. Lett. 30, 10–18.

Clenet, H., Jutzi, M., Barrat, J.A., Asphaug, E.I., Benz, W., Gillet, P., 2014. A deep crust–mantle boundary in the asteroid 4 Vesta. Nature 511, 303–306.

Connelly, J.N., Bizzarro, M., Krot, A.N., Nordlund, Å., Wielandt, D., Ivanova, M.A., 2012. The absolute chronology and thermal processing of solids in the solar protoplanetary disk. Science 338, 651–655.

Consolmagno, G.J., Drake, M.J., 1977. Composition and evolution of the eucrite parent body: evidence from rare earth elements. Geochim. Cosmochim. Acta 41, 1271–1282.

De Sanctis, M.C., Ammannito, E., Capria, M.T., Tosi, F., Capaccioni, F., Zambon, F., Carraro, F., Frigeri, A., Jaumann, R., Magni, G., Marchi, S., McCord, T.B., McFadden, L.A., McSween, H.Y., Mittlefehldt, D.W., Nathues, A., Palomba, E., Pieters, C.M., Raymond, C.A., Russell, C.T., Toplis, M.J., Turrini, D., 2012. Spectroscopic characterization of mineralogy and its diversity across Vesta. Science 336, 697–700.

Drake, M.J., 2001. The eucrite/Vesta story. Meteorit. Planet. Sci. 36, 501–513.

Duke, M.B., Silver, L.T., 1967. Petrology of eucrites, howardites and mesosiderites. Geochim. Cosmochim. Acta 31, 1637–1665.

El Goresy, A., Ramdohr, P., 1975. Subsolidus reduction of lunar opaque oxides: textures, assemblages, geochemistry, and evidence for a late-stage endogenic gaseous mixture. Proc. Lunar Planet. Sci. Conf. 6, 729–745.

Ewing, T.A., Hermann, J., Rubatto, D., 2013. The robustness of the Zr-in-rutile and Ti-in-zircon thermometers during high-temperature metamorphism (Ivrea-Verbano Zone, northern Italy). Contrib. Mineral. Petrol. 165, 757–779.

Ferriss, E.D.A., Essene, E.J., Becker, U., 2008. Computational study of the effect of pressure on the Ti-in-zircon thermometer. Eur. J. Mineral. 20, 745–755.

Ferry, J.M., Watson, E.B., 2007. New thermodynamic models and revised calibrations for the Ti-in-zircon and Zr-in-rutile thermometers. Contrib. Mineral. Petrol. 154, 429–437.

Fu, B., Page, F.Z., Cavosie, A.J., Fournelle, J., Kita, N.T., Lackey, J.S., Wilde, S.A., Valley, J.W., 2008. Ti-in-zircon thermometry: applications and limitations. Contrib. Mineral. Petrol. 156, 197–215.

Fu, B., Mernagh, T.P., Kita, N.T., Kemp, A.I.S., Valley, J.W., 2009. Distinguishing magmatic zircon from hydrothermal zircon: a case study from the Gidginbung high-sulphidation Au–Ag–(Cu) deposit, SE Australia. Chem. Geol. 259, 131–142.

Ghent, E.D., Stout, M.Z., 1984. TiO_2 activity in metamorphosed politic and basic rocks: principles and applications to metamorphism in southeastern Canadian Cordillera. Contrib. Mineral. Petrol. 86, 248–255.

Glavin, D.P., Kubny, A., Jagoutz, E., Lugmair, G.W., 2004. Mn–Cr isotope systematics of the D'Orbigny angrite. Meteorit. Planet. Sci. 39, 693–700.

Grange, M.L., Nemchin, A.A., Timms, N., Pidgeon, R.T., Meyer, C., 2011. Complex magmatic and impact history prior to 4.1 Ga recorded in zircon from Apollo 17 South Massif aphanitic breccia 73235. Geochim. Cosmochim. Acta 75, 2213–2232.

Greenwood, R.C., Franchi, I.A., Jambon, A., Buchanan, P.C., 2005. Widespread magma oceans on asteroidal bodies in the early Solar System. Nature 435, 916–918.

Haba, M.K., Yamaguchi, A., Horie, K., Hidaka, H., 2014. Major and trace elements of zircons from basaltic eucrites: implications for the formation of zircons on the eucrite parent body. Earth Planet. Sci. Lett. 387, 10–21.

Harlov, D.E., Förster, J.-H., 2002. High-grade fluid metasomatism on both local and a regional scale: the Seward Peninsula, Alaska, and the Val Strona di Omegna, Ivrea–Verbano Zone, Northern Italy. Part I: Petrography and silicate mineral chemistry. J. Petrol. 43, 769–799.

Hayden, L.A., Watson, E.B., 2007. Rutile saturation in hydrous siliceous melts and its bearing on Ti-thermometry of quartz and zircon. Earth Planet. Sci. Lett. 258, 561–568.

Hiess, J., Nutman, A.P., Bennett, V.C., Holden, P., 2008. Ti-in-zircon thermometry applied to contrasting Archean metamorphic and igneous systems. Chem. Geol. 247, 323–338.

Hirata, T., 2001. Determinations of Zr isotopic composition and U–Pb ages for terrestrial and extraterrestrial Zr-bearing minerals using laser ablation-inductively coupled plasma mass spectrometry: implications for Nb–Zr isotopic systematics. Chem. Geol. 176, 323–342.

Hoskin, P.W.O., Ireland, T.R., 2000. Rare earth element chemistry of zircon and its use as a provenance indicator. Geology 28, 627–630.

Huyskens, M.H., Iizuka, T., Amelin, Y., 2012. Evaluation of colloidal silicagels for lead isotopic measurements using thermal ionisation mass spectrometry. J. Anal. At. Spectrom. 27, 1439–1446.

Ickert, R.B., Williams, I.S., Wyborn, D., 2011. Ti in zircon from the Boggy Plain zoned pluton: implications for zircon petrology and Hadean tectonics. Contrib. Mineral. Petrol. 162, 447–461.

Iizuka, T., Kaltenbach, A., Amelin, Y., Stirling, C.H., Yamaguchi, A., 2013. U–Pb isotope systematics of eucrites in relation to their thermal history. In: 44th Lunar and Planetary Science Conference. Abstract # 1907.

Iizuka, T., Amelin, Y., Kaltenbach, A., Koefoed, P., Stirling, C.H., 2014. U–Pb systematics of the unique achondrite Ibitira: precise age determination and petrogenetic implications. Geochim. Cosmochim. Acta 132, 259–273.

Ireland, T.R., Bukovanska, M., 1992. Zircons from the Stannern eucrite. Meteoritics 27, 273.

Ireland, T.R., Bukovanska, M., 2003. Initial $^{182}Hf/^{180}Hf$ in meteoritic zircons. Geochim. Cosmochim. Acta 132, 259–273.

Jaumann, R., Williams, D.A., Buczkowski, D.L., Yingst, R.A., Preusker, F., Hiesinger, H., Schmedemann, N., Kneissl, T., Vincent, J.B., Blewett, D.T., Buratti, B.J., Carsenty, U., Denevi, B.W., De Sanctis, M.C., Garry, W.B., Keller, H.U., Kersten, E., Krohn, K., Li, J.Y., Marchi, S., Matz, K.D., McCord, T.B., McSween, H.Y., Mest, S.C., Mittlefehldt, D.W., Mottola, S., Nathues, A., Neukum, G., O'Brien, D.P., Pieters, C.M., Prettyman, T.H., Raymond, C.A., Roatsch, T., Russell, C.T., Schenk, P., Schmidt, B.E., Scholten, F., Stephan, K., Sykes, M.V., Tricarico, P., Wagner, R., Zuber, M.T., Sierks, H., 2012. Vesta's shape and morphology. Science 336, 687–690.

Jurewicz, A.J.G., Mittlefehldt, D.W., Jones, J.H., 1993. Experimental partial melting of the Allende (CV) and Murchison (CV) chondrites and the origin of asteroidal basalts. Geochim. Cosmochim. Acta 57, 2123–2139.

Kaltenbach, A., 2013. Uranium isotopic analysis of terrestrial and extraterrestrial samples, PhD thesis. University of Otago.

Kleine, T., Mezger, K., Palme, H., Scherer, D., Münker, C., 2005. The W isotopic composition of eucrite metals: constraints on the timing and cause of the thermal metamorphism of basaltic eucrites. Earth Planet. Sci. Lett. 231, 41–52.

Kleine, T., Hans, U., Irving, A.J., Bourdon, B., 2012. Chronology of the angrite parent body and implications for core formation in protoplanets. Geochim. Cosmochim. Acta 84, 186–203.

Kunz, J., Trieloff, M., Bobe, K.D., Metzler, K., Stöffler, D., Jossberger, E.K., 1995. The collisional history of the HED parent body inferred from ^{40}Ar–^{39}Ar ages of eucrites. Planet. Space Sci. 43, 527–543.

Larson, H.P., Fink, U., 1975. Infrared spectral observations of Asteroid 4 Vesta. Icarus 20, 213–239.

Lugmair, G.W., Shukolyukov, A., 1998. Early solar system timescales according to ^{53}Mn–^{53}Cr systematics. Geochim. Cosmochim. Acta 62, 2863–2886.

Manhes, G., Allegre, C.J., Provost, A., 1984. U–Th–Pb systematics of the eucrite "Juvinas": precise age determination and evidence for exotic lead. Geochim. Cosmochim. Acta 48, 2247–2264.

McCord, T.B., Adams, J.B., Johnson, T.V., 1970. Asteroid Vesta: spectral reflectivity and compositional implications. Science 168, 1445–1447.

McDonough, W.F., Sun, S.-s., 1995. The composition of the Earth. Chem. Geol. 120, 223–253.

McSween, H.Y., Labotka, T.C., 1993. Oxidation during metamorphism of the ordinary chondrites. Geochim. Cosmochim. Acta 57, 1105–1114.

McSween, H.Y., Binzel, R.P., De Sanctis, M.C., Ammannito, E., Prettyman, T.H., Beck, A.W., Reddy, V., Le Corre, L., Gaffey, M.J., McCord, T.B., Raymond, C.A., Russell, C.T., the Dawn Science Team, 2013. Dawn; the Vesta–HED connection; and the geologic context for eucrites, diogenites, and howardites. Meteorit. Planet. Sci. 48, 2090–2104.

Metzler, K., Bobe, K.D., Palme, H., Spettel, B., Stöffler, D., 1995. Planet. Space Sci. 43, 499–525.

Misawa, K., Yamaguchi, A., Kaiden, H., 2005. U–Pb and ^{207}Pb–^{206}Pb ages of zircons from basaltic eucrites: implications for early basaltic volcanism on the eucrite parent body. Geochim. Cosmochim. Acta 69, 5847–5861.

Miyamoto, M., Takeda, H., 1977. Evaluation of a crust model of eucrites from the width of exsolved pyroxene. Geochem. J. 11, 161–169.

Miyamoto, M., Takeda, H., 1994. Evidence for excavation of deep crustal material of a Vesta-like body from Ca compositional gradients in pyroxene. Earth Planet. Sci. Lett. 122, 343–349.

Morisset, C.-E., Scoates, J.S., 2008. Origin of zircon rims around ilmenite in mafic plutonic rocks of Proterozoic anorthosite suites. Can. Mineral. 46, 289–304.

Naslund, H.R., 1987. Lamella of baddeleyite and Fe–Cr spinel in ilmenite from the Basistoppen sill, East Greenland. Can. Mineral. 25, 91–96.

Nemchin, A., Timms, N., Pidgeon, R., Geisler, T., Reddy, S., Meyer, C., 2009. Timing of crystallization of the lunar magma ocean constrained by the oldest zircon. Nat. Geosci. 2, 133–136.

Nyquist, L.E., Takeda, H., Bansal, B.M., Shih, C.-Y., Wiesmann, J., Wooden, J.L., 1986. Rb–Sr and Sm–Nd internal isochron ages of a subophitic basalt clast and a matrix sample from the Y75011 eucrite. J. Geophys. Res. 91, 8137–8150.

Nyquist, L., Bogard, D., Takeda, H., Bansal, B., Wiesmann, H., Shih, C.-Y., 1997. Crystallization, recrystallization, and impact-metamorphic ages of eucrites Y792510 and Y791186. Geochim. Cosmochim. Acta 61, 2119–2138.

Palme, H., Wlotzka, F., Spettel, B., Dreibus, G., Weber, H., 1988. Camel Donga: a eucrite with high metal content. Meteoritics 23, 49–57.

Pearce, N.J.G., Perkins, W.T., Westgate, J.A., Gorton, M.P., Jackson, S.E., Neal, C.R., Chenery, S.P., 1997. A compilation of new and published major and trace element data for NIST SRM 610 and NIST SRM 612 glass reference materials. Geostand. Newsl. 21, 115–144.

Righter, K., Drake, M.J., 1997. A magma ocean on Vesta: core formation and petrogenesis of eucrites and diogenites. Meteorit. Planet. Sci. 32, 929–944.

Roszjar, J., Metzler, K., Bischoff, A., Barrat, J.A., Geisler, T., Greenwood, R.C., Franchi, I.A., Klemme, S., 2011. Thermal history of Northwest Africa 5073—a coarse-grained Stannern-trend eucrite containing cm-sized pyroxenes and large zircon grains. Meteorit. Planet. Sci. 46, 1754–1773.

Roszjar, J., Srinivasan, G., Whitehouse, M., Bischoff, A., Mezger, K., 2012. Hf–W analyses of eucrite zircon: new crystallization timescale for the eucrite parent body. In: 43rd Lunar and Planetary Science Conference. Abstract # 1774.

Roszjar, J., Whitehouse, M.J., Bischoff, A., 2014. Meteoritic zircon — Occurrence and chemical characteristics. Chem. Erde 74, 453–469. http://dx.doi.org/10.1016/j.chemer.2014.05.002.

Russell, C.T., Raymond, C.A., Coradini, A., McSween, H.Y., Zuber, M.T., Nathues, A., De Sanctis, M.C., Jaumann, R., Konopliv, A.S., Preusker, F., Asmar, S.W., Park, R.S., Gaskell, R., Keller, H.U., Mottola, S., Roatsch, T., Scully, J.E.C., Smith, D.E., Tricarico, P., Toplis, M.J., Christensen, U.R., Feldman, W.C., Lawrence, D.J., McCoy, T.J., Prettyman, T.H., Reedy, R.C., Sykes, M.E., Titus, T.N., 2012. Dawn at Vesta: testing the protoplanetary paradigm. Science 336, 684–686.

Ruzicka, A., Snyder, G.A., Taylor, L.A., 1997. Vesta as the howardite, eucrite and diogenite parent body: implications for the size of a core and for large-scale differentiation. Meteorit. Planet. Sci. 32, 825–840.

Schiller, M., Baker, J.A., Bizzarro, M., 2010. ^{26}Al–^{26}Mg dating of asteroidal magmatism in the young Solar System. Geochim. Cosmochim. Acta 74, 4844–4864.

Schwartz, J.M., McCallum, I.S., 2005. Comparative study of equilibrated and unequilibrated eucrites: subsolidus thermal histories of Haraiya and Pasamonte. Am. Mineral. 90, 1871–1886.

Shearer, C.K., Burger, P.V., Guan, Y., Papike, J.J., Sutton, S.R., Atudorei, N.-Y., 2012. Origin of sulfide replacement textures in lunar breccias. Implications for vapor element transport in the lunar crust. Geochim. Cosmochim. Acta 83, 138–158.

Shukolyukov, A., Begemann, F., 1996. Pu–Xe dating of eucrites. Geochim. Cosmochim. Acta 60, 2453–2471.

Söderlund, P., Söderlund, U., 2004. Petrology and ion microprobe U–Pb chronology applied to a metabasic intrusion in southern Sweden: a study on zircon formation during metamorphism and deformation. Tectonics 23, TC5005.

Srinivasan, G., Goswami, J.N., Bhandari, N., 1999. ^{26}Al in eucrite Piplia Kalan: plausible heat source and formation chronology. Science 284, 1348–1350.

Srinivasan, G., Whitehouse, M.J., Weber, I., Yamaguchi, A., 2004. U–Pb and Hf–W chronometry of zircons from eucrite A881467. In: 35th Lunar and Planetary Science Conference. Abstract # 1709.

Srinivasan, G., Whitehouse, M.J., Weber, I., Yamaguchi, A., 2007. The crystallization age of eucrite zircon. Science 317, 345–347.

Stolper, E., 1977. Experimental petrology of eucritic meteorites. Geochim. Cosmochim. Acta 41, 587–611.

Takeda, H., Graham, A.L., 1991. Degree of equilibration of eucritic pyroxenes and thermal metamorphism of the earliest planetary crust. Meteoritics 26, 129–134.

Takeda, H., Mori, H., 1985. The diogenite–eucrite links and the crystallization history of a crust of their parent body. J. Geophys. Res. 90, c636–c648.

Taylor, D.J., McKeegan, K.D., Harrison, T.M., 2009. Lu–Hf zircon evidence for rapid lunar differentiation. Earth Planet. Sci. Lett. 279, 157–164.

Tera, F., Carlson, R.W., Boctor, N.Z., 1997. Radiometric ages of basaltic achondrites and their relation to the early history of the Solar System. Geochim. Cosmochim. Acta 61, 1713–1731.

Trail, D., Watson, E.B., Tailby, N.D., 2011. The oxidation state of Hadean magmas and implications for early Earth's atmosphere. Nature 480, 79–82.

Trail, D., Watson, E.B., Tailby, N.D., 2012. Ce and Eu anomalies in zircon as proxies for the oxidation state of magmas. Geochim. Cosmochim. Acta 97, 70–87.

Treiman, A.H., Lanzirotti, A., Xirouchakis, D., 2004. Ancient water on asteroid 4 Vesta: evidence from a quartz veinlet in the Serra de Magé eucrite meteorite. Earth Planet. Sci. Lett. 219, 189–199.

Trinquier, A., Birck, J.-L., Allegre, C.J., Göpel, C., Ulfbeck, D., 2008. ^{53}Mn–^{53}Cr systematics of the early Solar System revisited. Geochim. Cosmochim. Acta 72, 5146–5163.

Valley, J.W., Spicuzza, M.J., Ushikubo, T., 2014. Correlated $\delta^{18}O$ and [Ti] in lunar zircons: a terrestrial perspective for magma temperatures and water content on the Moon. Contrib. Mineral. Petrol. 167, 956.

Wänke, H., Baddenhausen, H., Dreibus, G., Jagoutz, E., Kruse, H., Palme, H., Spettel, G., Teschke, F., 1973. Multielement analyses of Apollo 15, 16, and 17 samples and the bulk composition of the Moon. Geochim. Cosmochim. Acta 2, 1461–1481.

Warren, P.H., 1985. Origin of howardites, diogenites and eucrites: a mass balance constraint. Geochim. Cosmochim. Acta 49, 577–586.

Warren, P.H., Rubin, A.E., Isa, J., Gessler, N., Ahn, I., Choi, B.-G., 2014. Northwest Africa 5738: multistage fluid-driven secondary alteration in an extraordinary evolved eucrite. Geochim. Cosmochim. Acta 141, 199–227.

Watson, E.B., Harrison, T.M., 2005. Zircon thermometer reveals minimum melting conditions on earliest Earth. Science 308, 841–844.

Watson, E.B., Wark, D.A., Thomas, J.B., 2006. Crystallization thermometers for zircon and rutile. Contrib. Mineral. Petrol. 151, 413–433.

Wiedenbeck, M., Hanchar, J.M., Peck, W.H., Sylvester, P., Valley, J., Whitehouse, M., Kronz, A., Morishita, Y., Nasdala, L., Fiebig, J., Franchi, I., Girard, J.-P., Greenwood, R.C., Hinton, R., Kita, N., Mason, P.R.D., Norman, M., Ogasawara, M., Piccoli, P.M., Rhede, D., Satoh, H., Schulz-Dobrick, B., Skår, Ø., Spicuzza, M.J., Terada, K., Tindle, A., Togashi, S., Vennemann, T., Xie, Q., Zheng, Y.F., 2004. Further characterisation of the 91500 zircon crystal. Geostand. Geoanal. Res. 28, 9–39.

Yamaguchi, A., Taylor, G.J., Keil, K., 1996. Global crustal metamorphism of the eucrite parent body. Icarus 124, 97–112.

Yamaguchi, A., Taylor, J., Keil, K., Floss, C., Crozaz, G., Nyquist, L.E., Bogard, D.D., Garrison, D.H., Reese, Y.D., Wiesmann, H., Shih, C.Y., 2001. Post-crystallization reheating and partial melting of eucrite EET90020 by impact into the host crust of asteroid 4 Vesta ∼4.50 Ga ago. Geochim. Cosmochim. Acta 65, 3577–3599.

Yamaguchi, A., Barrat, J.A., Greenwood, R.C., Shirai, N., Okamoto, C., Setoyanagi, T., Ebihara, M., Franchi, I.A., Bohn, M., 2009. Crustal partial melting on Vesta: evidence from highly metamorphosed eucrites. Geochim. Cosmochim. Acta 73, 7162–7182.

Yamaguchi, A., Mikouchi, T., Ito, M., Shirai, N., Barrat, J.A., Messenger, S., Ebihara, M., 2013. Experimental evidence of fast transport of trace elements in planetary basaltic crusts by high temperature metamorphism. Earth Planet. Sci. Lett. 368, 101–109.

Zhou, Q., Yin, Q.Z., Young, E.D., Li, X.H., Wu, F.Y., Li, Q.L., Liu, Y., Tang, G.Q., 2013. SIMS Pb–Pb and U–Pb age determination of eucrite zircons at <5 μm scale and the first 50 Ma of the thermal history of Vesta. Geochim. Cosmochim. Acta 110, 152–175.